Adsorption and Desorption of U(VI) on Functionalized Graphene Oxides: A Combined Experimental and Theoretical Study

ARTICLE *in* ENVIRONMENTAL SCIENCE AND TECHNOLOGY · MARCH 2015

Impact Factor: 5.33 · DOI: 10.1021/es505590j · Source: PubMed

6 AUTHORS, INCLUDING:

Yubing Sun
Hefei Institute of Physical Sciences, Chinese A…
40 PUBLICATIONS **794** CITATIONS
SEE PROFILE

Shubin Yang
Hokkaido University
11 PUBLICATIONS **360** CITATIONS
SEE PROFILE

Congcong Ding
Chinese Academy of Science, Hefei
18 PUBLICATIONS **160** CITATIONS
SEE PROFILE

Xiangke Wang
Chinese Academy of Sciences
297 PUBLICATIONS **13,301** CITATIONS
SEE PROFILE

Environmental Science & Technology

Article

pubs.acs.org/est

Adsorption and Desorption of U(VI) on Functionalized Graphene Oxides: A Combined Experimental and Theoretical Study

Yubing Sun,[†,⊥] Shubin Yang,[†] Yue Chen,*[,‡] Congcong Ding,[§] Wencai Cheng,[§] and Xiangke Wang*[,†]

[†]School of Environment and Chemical Engineering, North China Electric Power University, Beijing 102206, P. R. China

[§]Key Lab of New Thin Film Solar Cells, Institute of Plasma Physics, Chinese Academy of Sciences, P.O. Box 1126, Hefei, 230031 Anhui, P. R. China

[‡]Fukui Institute for Fundamental Chemistry, Kyoto University, Takano-Nishihiraki-cho 34-4, Sakyo-ku, Kyoto 606-8103, Japan

[⊥]Collaborative Innovation Center of Radiation Medicine of Jiangsu Higher Education Institutions, Suzhou, Jiangsu, P. R. China

Supporting Information

ABSTRACT: The adsorption and desorption of U(VI) on graphene oxides (GOs), carboxylated GOs (HOOC-GOs), and reduced GOs (rGOs) were investigated by batch experiments, EXAFS technique, and computational theoretical calculations. Isothermal adsorptions showed that the adsorption capacities of U(VI) were GOs > HOOC-GOs > rGOs, whereas the desorbed amounts of U(VI) were rGOs > GOs > HOOC-GOs by desorption kinetics. According to EXAFS analysis, inner-sphere surface complexation dominated the adsorption of U(VI) on GOs and HOOC-GOs at pH 4.0, whereas outer-sphere surface complexation of U(VI) on rGO was observed at pH 4.0, which was consistent with surface complexation modeling. Based on the theoretical calculations, the binding energy of $[G^{\cdots}UO_2]^{2+}$ (8.1 kcal/mol) was significantly lower than those of $[HOOC\text{-}GOs^{\cdots}UO_2]^{2+}$ (12.1 kcal/mol) and $[GOs\text{-}O^{\cdots}UO_2]^{2+}$ (10.2 kcal/mol), suggesting the physisorption of UO_2^{2+} on rGOs. Such high binding energy of $[GOs\text{-}COO^{\cdots}UO_2]^{+}$ (50.5 kcal/mol) revealed that the desorption of U(VI) from the −COOH groups was much more difficult. This paper highlights the effect of the hydroxyl, epoxy, and carboxyl groups on the adsorption and desorption of U(VI), which plays an important role in designing GOs for the preconcentration and removal of radionuclides in environmental pollution cleanup applications.

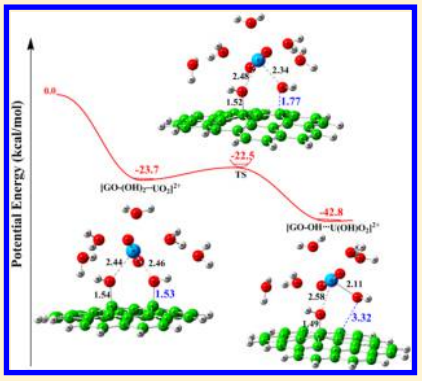

INTRODUCTION

Uranium contamination in groundwater is a continuing issue associated with the mining, milling, and processing of materials for the nuclear power industry.[1] Therefore, the safe treatment and disposal of radioactive wastes have been a public environmental concern.[2] The mobility of uranium in groundwater has been demonstrated to be primarily dependent on the adsorption of U(VI) at water-mineral interfaces.[3−5] Therefore, the rapid and effective adsorption of U(VI) from aqueous solutions by a variety of adsorbents with large adsorption capacities has been extensively investigated. The adsorption mechanism plays a vital role in the design of cost-effective remediation technologies and the development of materials suitable for the encapsulation and disposal of nuclear waste.[6]

Due to their unique chemical activities, excellent dispersive properties, and outstanding adsorption performances, graphene oxides (GOs) have been investigated as high efficient adsorbents to remove environmental contaminants.[7−15] Sun et al. found that the maximum adsorption capacity of a few layered GOs at pH 4.5 and 298 K was 175 mg/g for Eu(III).[9] The high adsorption capacity of GOs can be attributed to a variety of oxygenated functional groups such as the hydroxyl (−OH) and epoxy (−O−) groups on the basal plane and the carboxyl (−COOH) groups at the sheet edges.[16−19] Zhao et al.[20] investigated the adsorption of U(VI) on a few-layered GOs by using extended X-ray absorption fine structure (EXAFS), whereas the adsorption and desorption of U(V) on carboxylated GOs (HOOC-GOs) and reduced GOs (rGOs) were not observed. To the authors' knowledge, there are a few studies on the effect of different oxygenated functional groups on the adsorption or desorption of U(VI) onto/from GOs.[21] Density functional theory (DFT) has been shown to be a powerful and useful tool for describing and predicting the chemical and physical properties of graphene-based materials.[22−24] Wu et al.[25] investigated the bonding nature of U(VI) and −OH groups of GOs at the sheet edges based on DFT calculations. However, the chemical affinities between U(VI) and the −OH, −COOH, and −O− groups of GOs, especially −OH groups on the basal plane, remain ambiguous.

The objectives of this study are (1) to investigate the effect of −OH, −O−, and −COOH groups on the adsorption and desorption of U(VI) on/from GOs by batch techniques and (2) to demonstrate the chemical affinities of −OH, −O−, and

Received: November 17, 2014
Revised: March 5, 2015
Accepted: March 11, 2015
Published: March 11, 2015

DOI: 10.1021/es505590j
Environ. Sci. Technol. 2015, 49, 4255−4262

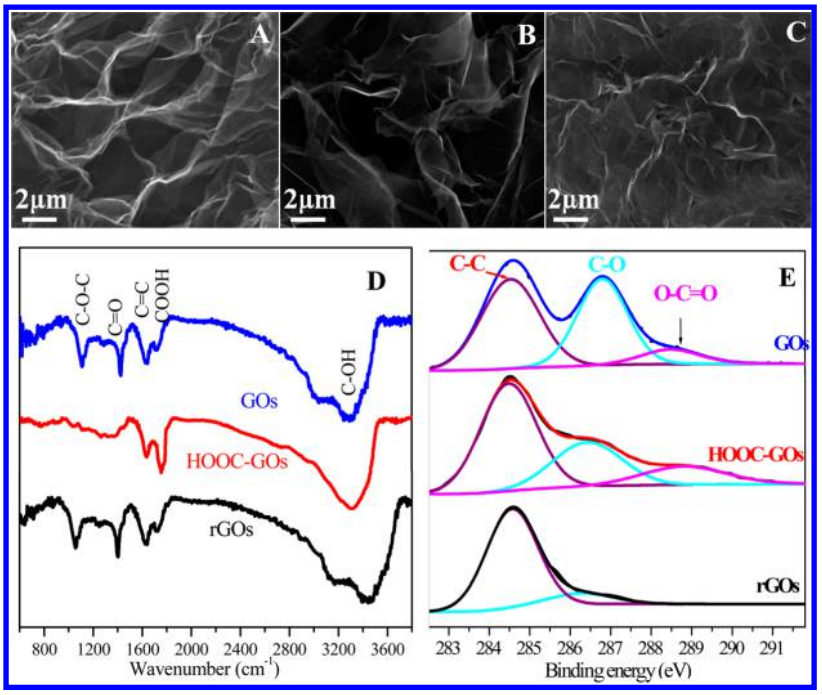

Figure 1. Characterization of GOs, HOOC-GOs, and rGOs. A-C: SEM images; D: FTIR; E: C 1s XPS.

−COOH groups with U(VI) by XPS, EXAFS, surface complexation modeling, and DFT calculations. This paper highlights the effect of various oxygenated functional groups on the removal and immobilization of radionuclides in aqueous solutions.

EXPERIMENTAL SECTION

Materials. Expanded graphite (<20 μm, 99.99% purity, QingDao Tianhe Graphite Co., Ltd.) was used as a starting material to ensure more uniform oxidization.[26−28] The ash content of the expanded graphite, as determined by TGA on a TASDT 2960 analyzer working under an air flow of 100 mL/min, was lower than 0.1 wt %. All chemicals, including concentrated H_2SO_4, $NaNO_3$, $KMnO_4$, H_2O_2 (37 wt %), $ClCH_2COONa$, and $NaBH_4$, were purchased as analytical reagents from Sinopharm Chemical Reagent Co., Ltd. The U(VI) stock solution (0.1 mol/L) was prepared from uranium nitrate ($UO_2(NO_3)_2{\cdot}6H_2O$, 99.99% purity, Sigma-Aldrich) after dissolution and dilution with Milli-Q water.

Fabrication of GOs, HOOC-GOs, and rGOs. GOs were obtained via the oxidation of expanded graphite by the modified Hummers method.[29] HOOC-GOs were synthesized by the chemical reduction of as-prepared GOs with $ClCH_2COONa$ under 1.25 mol/L NaOH solutions,[28,30,31] whereas rGOs were fabricated by $NaBH_4$ reduction under reflux condenser conditions.[32,33] More detailed processes on the synthesis of GOs, HOOC-GOs, and rGOs are described in the Supporting Information (SI). The elemental compositions, zeta-potential, S_{BET}, and the contents of various oxygenated functional groups of as-prepared GO, HOOC-GOs, and rGOs were summarized in Table S1.

Characterization. The as-prepared GOs, HOOC-GOs, and rGOs were characterized by using SEM (FEI Philips XL30 FEG scanning electron microscope), FTIR (PerkinElmer Spectrum 100 system spectrometer), XPS (Thermo ESCALAB 250 electron spectrometer), Raman spectroscopy (LabRam HR Raman spectrometer), and EXAFS techniques (Shanghai Synchrotron Radiation Facility). The SEM samples were prepared by dispensing a small amount of suspension on a 1 × 1 cm section of silicon wafer. The FTIR spectra of the samples were recorded in pressed KBr pellets (Aldrich, 99%, analytical reagent) at room temperature. The XPS spectra of the samples were conducted at 10 kV and 5 mA under 10^{-8} Pa residual pressure. The peak energies were corrected with C 1s peak at 284.6 eV as a reference. The recorded lines (C 1s, O 1s, and U 4f) were fitted using the XPSPEAK41 program after the background subtraction (i.e., a Shirley baseline correction). The Raman measurement was conducted with excitation at 514.5 nm for only 10 s by Ar^+ laser to avoid overheating of the GOs films. The EXAFS spectra of samples were collected in fluorescence mode with a silicon (111) double-crystal monochromator. The analyses and fitting of the EXAFS data were performed using the Athena and Artemis interfaces of the IFFEFIT 7.0 software.[34] More details on the preparation and analyses of EXAFS are provided in the SI.

Batch Adsorption and Desorption Experiments. The effect of pH and ionic strength on the adsorption of U(VI) onto GOs, HOOC-GOs, and rGOs (0.25 g/L) were examined at 293 K conditions using batch technique. The pH of suspension was adjusted with 0.01−1.0 mol/L $HClO_4$ or NaOH solution. Owing to the actual nuclear wastewater solutions at very low pH values,[12] therefore adsorption isotherms were investigated at pH 4.0 within a concentration range of 1 to 100 mg/L. Briefly, the bulk suspensions of GOs, HOOC-GOs, and rGOs and $NaClO_4$ (as nonreactive electrolyte) were pre-equilibrated for 24 h, then U(VI) stock solutions were spiked into bulk suspension gradually, and then the pH value of the suspension was adjusted to pH 4.0 with 0.01−1.0 mol/L $HClO_4$ and/or NaOH solution. Subsequently, the suspensions were shaken for 48 h to ensure that the adsorption reaction could achieve adsorption equilibrium. To eliminate the effect of U(VI) adsorption on polycarbonate tube walls, the adsorption of U(VI) without adsorbents was also carried out under the same experimental conditions.

DOI: 10.1021/es505590j
Environ. Sci. Technol. 2015, 49, 4255−4262

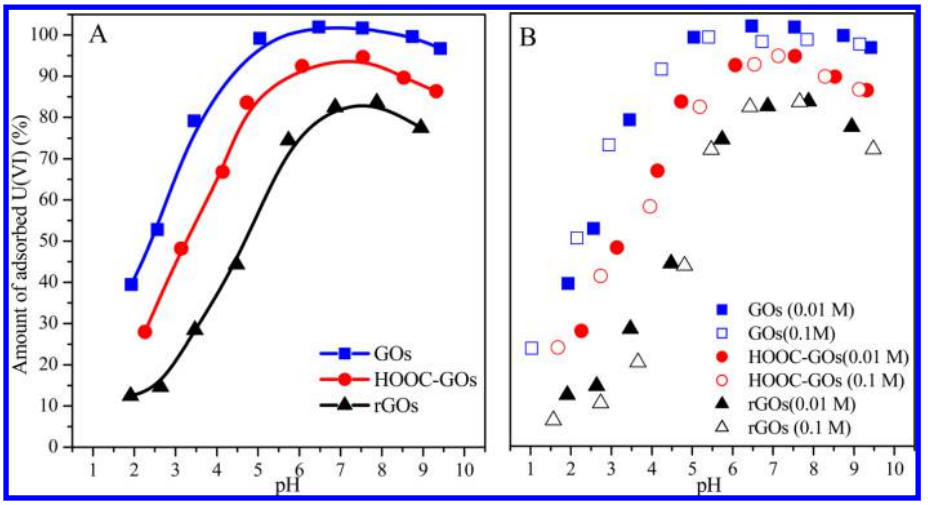

Figure 2. A: The effect of pH on U(VI) adsorption onto GOs, HOOC-GOs, and rGOs, $C_{[UO_2^{2+}]}$ = 60.0 mg/L, m/v = 0.25 g/L, T = 293 K, I = 0.01 mol/L $NaClO_4$. B: The effect of ionic strength on U(VI) adsorption onto GOs, HOOC-GOs, and rGOs, $C_{[UO_2^{2+}]}$ = 60.0 mg/L, m/v = 0.25 g/L, T = 293 K.

The desorption kinetics of U(VI) from GOs, HOOC-GOs, and rGOs were investigated after adsorption equilibrium by using $NaClO_4$ solution. Briefly, 3.0 mL of supernatant after adsorption equilibrium was removed, and then 3.0 mL of 0.01 mol/L of $NaClO_4$ solution was added into the uranium-containing GOs, HOOC-GOs, or rGOs. The pH of the suspension was adjusted to pH 4.0 with 0.01−1.0 mol/L $HClO_4$ solution, and then aforementioned suspension was reacted at different reaction times (from 5 min to 24 h) and under continuous stirring conditions. The solid and liquid phases were separated by centrifugation at 7104 × g for 30 min, and then the supernatant was separated by using 0.22-μm membrane filters. More details on the batch adsorption and desorption experiments are provided in the SI. The concentration of U(VI) was analyzed by a kinetic phosphorescence analyzer (KPA-11, Richland, USA). All experimental data were averaged from three independent measurements, and 5% error bars were provided.

Computational Details. To understand the interactions of U(VI) with the −OH, −O−, and −COOH groups, a series of finite-sized computational models were analyzed (Figure S1 in the SI). A pentacoordinated uranyl species ($[UO_2(H_2O)_5]^{2+}$, the first sovation shell of a uranyl dication with an average of five ligands in equatorial positions) was the dominant species in aqueous solution;[25] therefore $[UO_2(H_2O)_5]^{2+}$ species was used in this study. The most stable structures of UO_2^{2+} with GOs were obtained by calculating the binding energies of U(VI) and the GOs ($E_{bd} = E_{(GOs)} + E_{([UO_2(H_2O)_5]^{2+})} - E_{[GOs\cdots UO_2(H_2O)_5]_{2+}}$) by DFT calculation with the Gaussian 09 package[35] and the PBE1PBE functional.[36] For geometric optimizations, the effective core potentials and basis set by the Stuttgart-Dresden-Bonn group were used for uranium atoms, while the cc-pVDZ was used for C, O, and H atoms.[37] A conductor polarized continuum model was also employed to consider the solvent effect in the geometric optimization.[38,39]

RESULTS AND DISCUSSION

Characterization. The morphologies of GOs, HOOC-GOs, and rGOs are visualized using SEM (Figure 1). As shown in Figure 1A-C, wrinkled and aggregated nanosheets were observed, which were consistent with previous studies.[40] The crumpled and overlaid nanosheets of GOs, HOOC-GOs, and rGOs indicated that multilayer nanosheets were formed. As shown in the FTIR spectra in Figure 1D, the as-prepared GOs presented the various oxygenated functional groups, such as −OH (broad peak at approximately 3450 cm^{-1}), −COOH (at approximately 1750 cm^{-1}), and −O− groups (at approximately 1050 cm^{-1}).[18,41] The broad peak at approximately 3450 cm^{-1} was assigned as stretching vibration of adsorbed water. The peak at 1600 cm^{-1} was attributed to the skeletal vibrations of nonoxidized graphitic domains.[42] The sharp peaks centered at 1400 cm^{-1} indicated −OH deformation vibrations.[42,43] The enhanced relative intensities at approximately 1750 cm^{-1} was observed for HOOC-GOs, which indicated an increased C═O stretching vibration in the −COOH groups.[44] However, the peaks at 1050 and 1400 cm^{-1} were severely attenuated in HOOC-GOs, which indicated that most of the −O− and −OH groups were removed by chemical reduction. For the rGOs nanosheets, the relative intensities of the peaks at approximately 3450, 1750, 1400, and 1050 cm^{-1} were significantly lower than those in GOs nanosheets, which indicated the significant removal of oxygenated functional groups through $NaBH_4$ reduction. The interpretation of the FTIR spectra indicated that the −OH and −O− groups of GOs can be replaced with −COOH groups by chemical reduction using $ClCH_2COONa$ under strong basic conditions, whereas a significant amount of oxygenated functional groups were removed by $NaBH_4$ reduction under reflux condenser conditions. Figure 1E showed the deconvoluted C 1s XPS spectra of GOs, HOOC-GOs, and rGOs. The GOs presented two separate peaks, as expected, due to the high percentage of oxygenated functionalities, whereas the rGOs and HOOC-GOs samples showed a single peak with broad tails in the higher binding energy region. The GOs spectra indicated the presence of sp^2-hybridized carbons in C−C at 284.5 eV, −OH/−O− groups at 286.6 eV, and −COOH groups at 289.0 eV.[45−47] The decreased relative intensities of the −OH/−O− groups at 286.6 eV were observed for the rGOs and HOOC-GOs samples, whereas the relative intensity of −COOH increased for HOOC-GOs. The XPS spectra showed that the significant numbers of −O− and −OH groups were replaced with −COOH groups.[46,48] This finding was further demonstrated by

DOI: 10.1021/es505590j
Environ. Sci. Technol. 2015, 49, 4255−4262

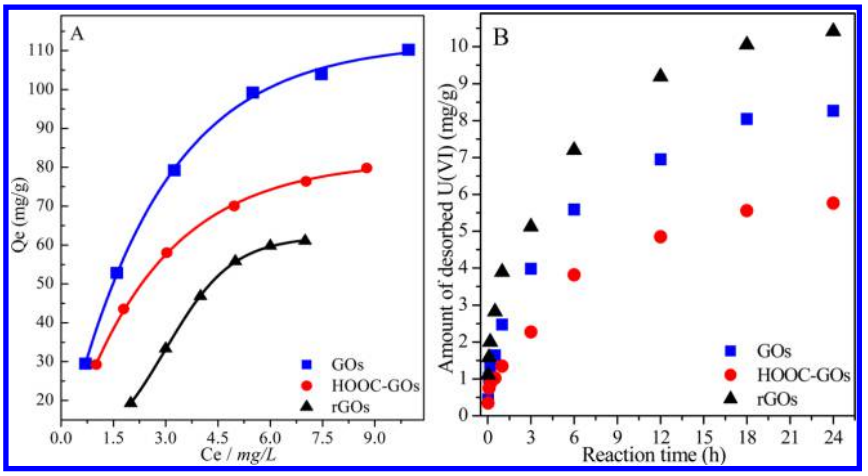

Figure 3. A: The adsorption isotherms of U(VI) on GOs, HOOC-GOs, and rGOs, pH = 4.0, m/v = 0.25 g/L, T = 293 K, I = 0.01 mol/L $NaClO_4$. B: The desorption kinetics of U(VI) on GOs, HOOC-GOs, and rGOs, pH = 4.0, $C_{[NaClO_4]}$ = 0.01 mol/L, m/v = 0.25 g/L, T = 293 K.

the contents of oxygenated functional groups calculated from the fitting O 1s of XPS spectra. As shown in Table S1, the contents of −OH (15.25 wt %) and −O− groups (6.93 wt %) of GOs were higher than those of HOOC-GOs (4.64 wt % of −OH and 3.38 wt % of −O− groups) and rGOs (2.95 wt % of −OH and 2.26 wt % of −O− groups), whereas the content of −COOH groups of HOOC-GOs (8.18 wt %) was significantly higher than those of GOs (1.72 wt %) and rGOs (0.55 wt %). The Raman spectra of GOs, HOOC-GOs, and rGOs samples displayed a D-band (i.e., disordered sp^3-hybridized carbons resulted from oxygenated functional groups) at approximately 1350 cm^{-1} and a broad G-band (i.e., graphitic sp^2-hybridized carbon) at approximately 1580 cm^{-1} (Figure S2A). The significant blue shift of the G-band (from 1584 cm^{-1} of rGOs to 1591 cm^{-1} of HOOC-GOs) revealed the gradual reduction of GOs.[49,50] The prominent D peak was attributed to the structural defects created by the attachment of −OH and −O− groups on the carbon basal plane.[51] Therefore, the ratio of the integrated intensities of the D- and G-bands (I_D/I_G) represents the oxidation degree and the size of the sp^2 ring clusters in a network of sp^3 and sp^2-bonded carbon.[52] The I_D/I_G values significantly decreased from 0.962 for GOs to 0.904 for rGOs, which suggested that a significant number of massive oxygenated functional groups were removed by chemical reduction.

The BET specific surface areas of GOs, HOOC-GOs, and rGOs were 140.8, 156.7, and 113.5 m^2/g, respectively, which were significantly below the theoretical values of a single-layered GOs (2700 m^2/g). These observations were likely due to the collapse of the nanosheets into relatively large and dense aggregates upon drying.[53] Based on the characterization results, a significant number of the −OH and −O− groups was reduced with −COOH groups by $ClCH_2COONa$ reduction under strong basic conditions, whereas the most oxygenated functional groups were removed by $NaBH_4$ reduction.

Effect of pH and Ionic Strength. Figure 2A shows the effect of pH on U(VI) adsorption on GOs, HOOC-GOs, and rGOs. As pH increased from 2.0 to 6.0, the adsorption of U(VI) on GOs, HOOC-GOs, and rGOs increased and maintained this maximum adsorption level for pH levels 6.0−8.0. However, the decreased adsorption was observed at pH levels above 8.0. As shown in Table S1, the zeta potential of GOs and HOOC-GOs at pH 2.0 were calculated to be −15.1 and −21.9 mV, respectively, indicating HOOC-GOs and GOs were highly negatively charged throughout wide range of pH.[54,55] However, the positive value of zeta potential of rGOs was observed at pH < 6.0. As shown in Figure S3, the positive-charge of the U(VI) species (e.g., UO_2^{2+}, UO_2OH^+, and $(UO_2)_3(OH)_5^+$) were observed at pH < 6.0. Therefore, the enhanced adsorption of U(VI) on GOs and HOOC-GOs at pH 2.0−6.0 can be attributed to electrostatic attraction between negatively charged GOs and positive-charge of U(VI) species, whereas lower adsorption of U(VI) on rGOs could be due to the electrostatic repulsion between positive charged GOs and positive-charge of U(VI) species. The observed decreased adsorption of U(VI) on GOs, HOOC-GOs, and rGOs at pH above 8.0 was due to the electrostatic repulsion between the negatively charged U(VI) species (e.g., $(UO_2)_3(OH)_7^-$ and $UO_2(OH)_3^-$ species) and the negatively charged GOs.[12] The effect of ionic strength on U(VI) adsorption onto GOs, HOOC-GOs, and rGOs was elucidated by batch technique (Figure 2B). As shown in Figure 2B, the slight effect of ionic strength on the adsorption of U(VI) onto GOs, HOOC-GOs, and rGOs was observed at pH > 4.0. It is demonstrated that the outer-sphere surface complexation was strongly sensitive to ionic strength, whereas inner-sphere surface complexation was independent of ionic strength.[56−58] Therefore, the adsorption of U(VI) on GOs, HOOC-GOs, and rGOs at pH > 4.0 was mainly dominated by inner-sphere surface complexation.

Adsorption and Desorption. The adsorption isotherms of U(VI) on GOs, HOOC-GOs, and rGOs were conducted at pH 4.0 and 293 K. As shown in Figure 3A, the adsorption of U(VI) on GOs, HOOC-GOs, and rGOs significantly increased with increasing initial concentrations. The adsorption amounts of U(VI) increased in the order of GOs > HOOC-GOs > rGOs, which indicated that GOs presented the higher adsorption capacity for U(VI) as compared to HOOC-GOs and rGOs. As shown in Table S1, the oxygen content of GOs (37.43 wt %) was significantly higher than that of rGOs (7.35 wt %), which was comparable to the results of Robinson et al., who reported that the oxygen content of GOs decreased from approximately 28.5% to 7.0% after chemical reduction.[59] The decreased oxygen content of HOOC-GOs (23.74%) was due to the fact that certain amounts of −O− and −OH groups were reduced.[60] The low oxygen content of rGOs indicated that most oxygenated functional groups were completely removed by $NaBH_4$ reduction. Therefore, the high adsorption of U(VI) on GOs could be attributed to the significant amount of

DOI: 10.1021/es505590j
Environ. Sci. Technol. 2015, 49, 4255−4262

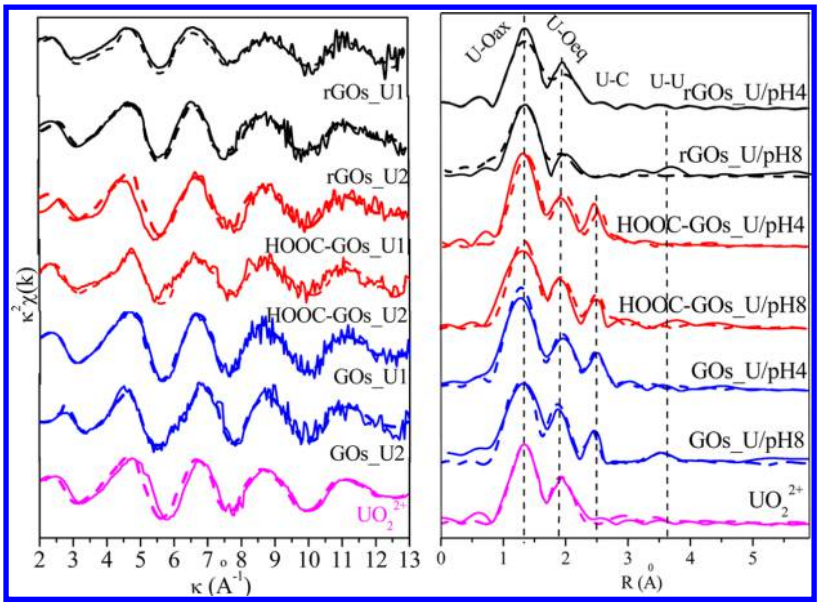

Figure 4. K^2-weighted U L_{III}-edge EXAFS spectra (A) and the corresponding Fourier Transforms (B) of the reference and samples before and after desorption, m/V = 0.25 g/L, $C_{[UO_2^{2+}]}$ = 60.0 mg/L, I = 0.01 mol/L $NaClO_4$, T = 293 K.

oxygenated functional groups and its excellent dispersive properties, which provided more available reaction sites for adsorption. The excellent dispersive property of GOs was due to the weaker stacking interactions and strong electrostatic repulsion between negatively charged sheets, confirmed by their negative zeta potential.[61] The adsorption of U(VI) on GOs, HOOC-GOs, and rGOs were characterized by Langmuir and Freundlich models, and their corresponding parameters were tabulated in Table S3. The maximum adsorption capacities of GOs, HOOC-GOs, and rGOs, as calculated from the Langmuir model at pH 4.0 and 293 *K*, were 138.89, 103.09, and 74.07 mg/g, respectively (Table S3), which were significantly greater than those of any known natural adsorbents such as hematite (1.0 mg/g at pH 4.0 and 0.1 mol/L $NaNO_3$),[62] montmorillonite (5.0 mg/g at pH 7.0 and 1.0 mol/L $NaNO_3$),[63] nanoporous alumina (11.6 mg/g at pH 4.5 and 0.01 mol/L $NaNO_3$).[64]

Figure 3B shows the desorption kinetics of U(VI) on GOs, HOOC-GOs, and rGOs in the presence of 0.01 mol/L $NaClO_4$ solution. The amount of desorbed U(VI) from GOs, HOOC-GOs, and rGOs significantly increased with increasing reaction time, especially within 3 h of reaction time. The desorbed amount of U(VI) significantly decreased in the order of rGOs > GOs > HOOC-GOs, which indicated that it was difficult to extract U(VI) from HOOC-GOs as compared to GOs.

EXAFS Analysis. Figure 4 shows the k^2-weighted U L_{III}-edge EXAFS spectra and the corresponding Fourier transforms (FT, uncorrected phase shift) of UO_2^{2+} and U(VI) adsorbed on GOs, HOOC-GOs, and rGOs at pH 4.0 and 8.0. As shown in Figure 4A, the EXAFS spectra of UO_2^{2+} species showed a distinct cyclic evolution, whereas a poor signal-to-noise ratio was observed for all samples at $\kappa > 8$ Å^{-1} due to the existence of low U(VI) concentration. Similar EXAFS spectra features were observed for GOs and HOOC-GOs (Figure 4B), whereas the FT features of rGOs were significantly different from those of GOs. The fitted results are also shown in Figure 4B (dashed lines), and the corresponding parameters are summarized in Table 1. The bond distance (R + ΔR) in the FT peaks at approximately 1.3 and 1.9 Å can be satisfactorily fitted by two

Table 1. EXAFS Results of Reference Samples and U(VI)-Reacted GOs at L_{III}-Edge, T = 293 K, I = 0.01 mol/L $NaClO_4$

samples	shell	R (Å)[a]	CN[b]	σ^2 (Å^2)[c]
UO_2^{2+}	U−O_{ax}	1.826(0)	2.0(0)	0.00180
	U−O_{eq}	2.577(1)	6.2(7)	0.00513
rGOs/pH 4.0	U−O_{ax}	1.825(2)	2.0(0)	0.00309
	U−O_{eq}	2.535(2)	4.9(9)	0.00834
rGOs/pH 8.0	U−O_{ax}	1.8264(1)	2.0(0)	0.00393
	U−O_{eq}	2.5140(6)	4.0(0)	0.00327
	U−U	3.9348 (7)	0.5(7)	0.02423
HOOC-GOs/pH 4.0	U−O_{ax}	1.7874(6)	2.0(0)	0.00381
	U−O_{eq}	2.5140(6)	4.5(9)	0.00592
	U−C	3.2308(1)	1.1(3)	0.01050
HOOC-GOs/pH 8.0	U−O_{ax}	1.7807(2)	2.0(0)	0.00431
	U−O_{eq}	2.3950(5)	4.2(2)	0.00970
	U−C	2.913(1)	1.2(1)	0.01942
	U−U	3.931(7)	0.2(4)	0.08432
GOs/pH 4.0	U−O_{ax}	1.8253(1)	2.0(0)	0.00545
	U−O_{eq}	2.4446(0)	4.2(3)	0.00627
	U−C	3.3100(7)	1.7(8)	0.07642
GOs/pH 8.0	U−O_{ax}	1.8088(0)	2.0(0)	0.00483
	U−O_{eq}	2.4532(0)	4.1(3)	0.00942
	U−C	2.9544(1)	1.7(8)	0.06321
	U−U	3.9242(1)	0.3(1)	0.08532

[a]R is the bond distance. [b]CN is coordination numbers of neighbors. [c]σ^2 is the Debye−Waller factor.

axial oxygen atoms (U-Oax at 1.8 Å) and approximately 4.5 equatorial oxygen atoms (U-Oeq, at approximately 2.30−2.50 Å), respectively, which in turn revealed O═U═O transdioxo structure.[62] The attempt to fit an equatorial U-Oeq shell into two subshells (U-Oeq1 and U-Oeq2) led to the convergence of two subshells at the same bond distance. For samples of GOs and HOOC-GOs, the FT peak at approximately 2.3 Å (Figure 4B) can be satisfactorily fitted by a U−C shell at 2.9 Å (Table 1),[65,66] whereas the fitting of rGOs by a U−C shell at approximately 2.9 Å was not be observed. The FT peaks of

DOI: 10.1021/es505590j
Environ. Sci. Technol. 2015, 49, 4255−4262

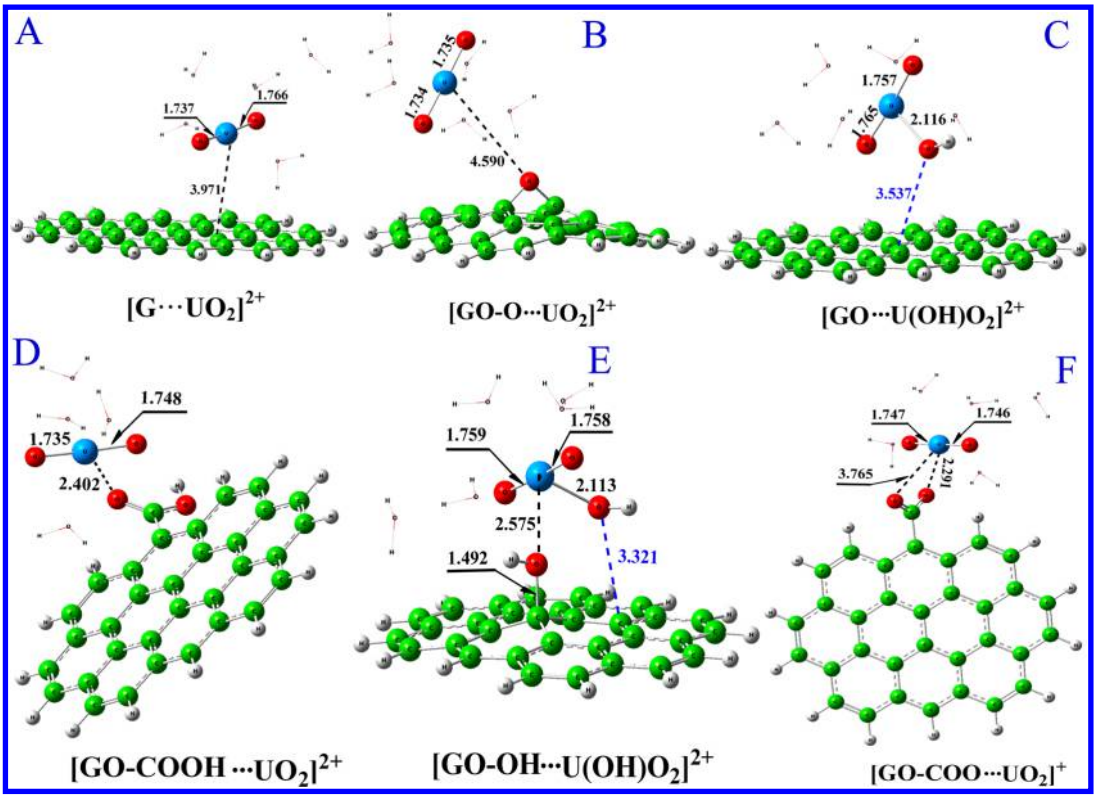

Figure 5. DFT-optimized geometries of the rGOs_uranyl complexes and GOs_uranyl complexes.

GOs-U/pH 8.0, HOOC-GOs-U/pH 8.0, and rGOs-U/pH 8.0 at approximately 3.6 Å could be fitted by a U−U shell at 3.9 Å (Table 1). This observation correlates with results reported by Bargar et al.[63] The presence of a U−U shell indicated that the adsorption of U(VI) on GOs, HOOC-GOs, and rGOs was ascribed to a coprecipitation at high pH conditions. The results from the EXAFS spectra showed that the primary inner-sphere surface complexation dominated the adsorption of U(VI) on GOs and HOOC-GOs, whereas the adsorption of U(VI) on rGOs was dominated by outer-sphere surface complexation at pH 4.0. The adsorption of U(VI) on GOs, HOOC-GOs, and rGOs was coprecipitation at high pH conditions.

The interaction mechanism of U(VI) on GOs, HOOC-GOs, and rGOs was also demonstrated by XPS analysis (Figure S5) and surface complexation modeling (Figure S6). According to XPS analysis, the high adsorption capacity of GOs for U(VI) was attributed to a variety of oxygenated functional groups such as −OH, −O−, and −COOH groups, whereas the chemical affinity of U(VI) with −COOH groups was stronger than that of U(VI) with −OH groups. The adsorption of U(VI) on GOs and HOOC-GOs can be satisfactorily fitted by using diffuse layer model with the strong (SsOH) and weak (SwOH) sites, whereas the adsorption of U(VI) on rGOs can be fitted by cation exchange (XH) and surface complexation (SOH) sites (Table S4). We tried to fit the adsorption of U(VI) on rGOs by using SsOH and SwOH sites, whereas the fitted results were not convergent. The fitted results indicated that the adsorption of U(VI) on GOs and HOOC-GOs were primary inner-sphere surface complexation, whereas the U(VI) adsorption on rGOs was outer-sphere surface complexation. As shown in Figure S6, approximately 75% and 55% of $SsOUO_2^+$ species were observed for HOOC-GOs and GOs at pH 7.0, respectively, which further corroborated the more strong sites of HOOC-GOs.

DFT Calculation. As shown in Figure 5, $[G^{\cdots}UO_2]^{2+}$, $[GOs\text{-}O^{\cdots}UO_2]^{2+}$, and $[HOOC\text{-}GOs^{\cdots}\ UO_2]^{2+}$ adducts presented UO_2^{2+} bonded with rGOs, −O− of GOs, and HOOC-GOs, respectively. It has been demonstrated that massive −OH groups were presented on the basal plane of GOs,[16−19] whereas these −OH groups were easily abstracted by UO_2^{2+} in aqueous solutions in terms of DFT calculation. Therefore, the $[GOs\text{-}U(OH)O_2]^{2+}$ and $[GOs{-}OH^{\cdots}\ U(OH)O_2]^{2+}$ adducts were also considered. This finding was significantly different from the previous study due to −OH groups of GOs at the sheet edges used.[25] The $[GO{-}COO^{\cdots}UO_2]^{2+}$ adduct was also considered due to the deprotonation of the −COOH group at high pH. As shown in Table S5, the binding energy (E_{bd}) of $[HOOC\text{-}GOs\cdots UO_2]^{2+}$ (12.1 kcal/mol) was greater than that of $[GOs\text{-}O\cdots UO_2]^{2+}$ (10.2 kcal/mol), which suggested that UO_2^{2+} was favored to bind with the −COOH group over the −O− group. The low E_{bd} value of $[G\cdots UO_2]^{2+}$ (8.1 kcal/mol) indicated that the adsorption of U(VI) on rGOs was a physical adsorption (8 kcal/mol).[67,68] The higher E_{bd} values of $[GOs^{\cdots}U(OH)O_2]^{2+}$ (45.5 kcal/mol) and $[GOs{-}OH^{\cdots}\ U(OH)O_2]^{2+}$ (42.8 kcal/mol) were attributed to the OH-abstraction from GOs, resulting in the chemical adsorption of U(VI) on GOs and HOOC-GOs. The E_{bd} of $[GOs\text{-}COO^{\cdots}UO_2]^+$ (50.5 kcal/mol) was significantly higher than those of $GOs^{\cdots}U(OH)O_2]^{2+}$ and $[GOs{-}OH^{\cdots}U(OH)O_2]^{2+}$, indicating that the desorption of U(VI) from the −COOH groups was much more difficult compared with that from −OH groups. The results of DFT calculation were consistent with the observations from the macroscopic experiments.

In the near future, GOs may be synthesized in large scale and at low price with the development of technology. In conclusion, the results are important in designing functionalized GOs for the preconcentration and removal of radionuclides in environ-

DOI: 10.1021/es505590j
Environ. Sci. Technol. 2015, 49, 4255−4262

mental pollution cleanup and nuclear waste management applications.

■ ASSOCIATED CONTENT

Supporting Information

Additional characterization data of Raman, distribution of U(VI) species, XPS analysis, surface complexation modeling, and adsorption isotherms. This material is available free of charge via the Internet at http://pubs.acs.org.

■ AUTHOR INFORMATION

Corresponding Authors

*Phone: 86-551-65592788. Fax: 86-551-65591310. E-mail: xkwang@ipp.ac.cn (X.W.).

*E-mail: cysqxr@hotmail.com (Y.C.).

Notes

The authors declare no competing financial interest.

■ ACKNOWLEDGMENTS

Y. B. Sun and S. B. Yang contributed equally to this paper. We thank Prof. Jiaxing Li for favorable discussions. Financial support from 973 projects from the Ministry of Science and Technology of China (2011CB933700), the National Natural Science Foundation of China (21207135, 21207136, 21225730, and 91126020), the Anhui Provincial Natural Science Foundation (1408085MB28), the Scientific Research Grant of Hefei Science Center of CAS (2015SRG-HSC006 and 2015SRG- HSC009), and the Jiangsu Provincial Key Laboratory of Radiation Medicine and Protection and the Priority Academic Program Development of Jiangsu Higher Education Institutions are acknowledged.

■ REFERENCES

(1) Morrison, S. J.; Spangler, R. R. Extraction of uranium and molybdenum from aqueous solutions: a survey of industrial materials for use in chemical barriers for uranium mill tailings remediation. *Environ. Sci. Technol.* **1992**, *26*, 1922−1931.

(2) World Health Organization (WHO) *Depleted uranium: sources, exposure and health effects*; WHO: Geneva, 2001.

(3) Langmuir, D. Uranium solution-mineral equilibria at low temperatures with applications to sedimentary ore deposits. *Geochim. Cosmochim. Acta* **1978**, *42*, 547−569.

(4) Ching, K.; Daniel, H.; Langmuir, D. Adsorption of uranyl onto ferric oxyhydroxides: Application of the surface complexation site-binding model. *Geochim. Cosmochim. Acta* **1985**, *49*, 1931−1941.

(5) Sun, Y.; Li, J.; Wang, X. The retention of uranium and europium onto sepiolite investigated by macroscopic, spectroscopic and modeling techniques. *Geochim. Cosmochim. Acta* **2014**, *140*, 621−643.

(6) Bargar, J. R.; Reitmeyer, R.; Davis, J. A. Spectroscopic confirmation of Uranium(VI)−carbonato adsorption complexes on hematite. *Environ. Sci. Technol.* **1999**, *33*, 2481−2484.

(7) Zhao, G.; Li, J.; Ren, X.; Chen, C.; Wang, X. Few-layered graphene oxide nanosheets as superior sorbents for heavy metal ion pollution management. *Environ. Sci. Technol.* **2011**, *45*, 10454−62.

(8) Yang, S. T.; Chen, S.; Chang, Y.; Cao, A.; Liu, Y.; Wang, H. Removal of methylene blue from aqueous solution by graphene oxide. *J. Colloid Interface Sci.* **2011**, *359*, 24−29.

(9) Sun, Y.; Wang, Q.; Chen, C.; Tan, X.; Wang, X. Interaction between Eu(III) and Graphene Oxide Nanosheets investigated by batch and extended X-ray absorption fine structure spectroscopy and by modeling techniques. *Environ. Sci. Technol.* **2012**, *46*, 6020−6027.

(10) Zhang, F.; Zheng, B.; Zhang, J.; Huang, X.; Liu, H.; Guo, S.; Zhang, J. Horseradish peroxidase immobilized on graphene oxide: physical properties and applications in phenolic compound removal. *J. Phys. Chem. C* **2010**, *114*, 8469−8473.

(11) Romanchuk, A. Y.; Slesarev, A. S.; Kalmykov, S. N.; Kosynkin, D. V.; Tour, J. M. Graphene oxide for effective radionuclide removal. *Phys. Chem. Chem. Phys.* **2013**, *15*, 2321−2327.

(12) Sun, Y.; Shao, D.; Chen, C.; Yang, S.; Wang, X. Highly efficient enrichment of radionuclides on graphene oxide-supported polyaniline. *Environ. Sci. Technol.* **2013**, *47*, 9904−9910.

(13) Sitko, R.; Turek, E.; Zawisza, B.; Malicka, E.; Talik, E.; Heimann, J.; Gagor, A.; Feist, B.; Wrzalik, R. Adsorption of divalent metal ions from aqueous solutions using graphene oxide. *Dalton Trans.* **2013**, *42*, 5682−5689.

(14) Ding, C.; Cheng, W.; Sun, Y.; Wang, X. Determination of chemical affinity of graphene oxide nanosheets with radionuclides investigated by macroscopic, spectroscopic and modeling techniques. *Dalton Trans.* **2014**, *43*, 3888−3896.

(15) Wang, J.; Chen, Z. M.; Chen, B. L. Adsorption of polycyclic aromatic hydrocarbons by graphene and graphene oxide nanosheets. *Environ. Sci. Technol.* **2014**, *48*, 4817−4825.

(16) Lerf, A.; He, H. Y.; Forster, M.; Klinowski, J. Structure of graphite oxide revisited. *J. Phys. Chem. B* **1998**, *102*, 4477−4482.

(17) Eda, G.; Chhowalla, M. Chemically derived graphene oxide: towards large-area thin-film electronics and optoelectronics. *Adv. Mater.* **2010**, *22*, 2392−2415.

(18) Chen, D.; Feng, H.; Li, J. Graphene oxide: preparation, functionalization, and electrochemical applications. *Chem. Rev.* **2012**, *112*, 6027−6053.

(19) Compton, O. C.; Nguyen, S. T. Graphene oxide, highly reduced graphene oxide, and graphene: versatile building blocks for carbon-based materials. *Small* **2010**, *6*, 711−723.

(20) Zhao, G. X.; Wen, T.; Yang, X.; Yang, S. B.; Liao, J. L.; Hu, J.; Shao, D. D.; Wang, X. K. Preconcentration of U(VI) ions on few-layered graphene oxide nanosheets from aqueous solutions. *Dalton Trans.* **2012**, *41*, 6182−6188.

(21) Li, Z. J.; Chen, F.; Yuan, L. Y.; Liu, Y. L.; Zhao, Y. L.; Chai, Z. F.; Shi, W. Q. Uranium(VI) adsorption on graphene oxide nanosheets from aqueous solutions. *Chem. Eng. J.* **2012**, *210*, 539−546.

(22) Yang, S.; Chen, C.; Chen, Y.; Wang, D.; Wang, X. Competitive adsorption of Pb(II), Ni(II) and Sr(II) ions on graphene oxides: A combined experimental and theoretical study. *ChemPlusChem* **2015**, *80*, 480−484.

(23) Boukhvalov, D. W.; Katsnelson, M. I. Modeling of graphite oxide. *J. Am. Chem. Soc.* **2008**, *130*, 10697−10701.

(24) Boukhvalov, D. W. DFT modeling of the covalent functionalization of graphene: from ideal to realistic models. *RSC Adv.* **2013**, *3*, 7150−7159.

(25) Wu, Q. Y.; Lan, J. H.; Wang, C. Z.; Xiao, C. L.; Zhao, Y. L.; Wei, Y. Z.; Chai, Z. F.; Shi, W. Q. Understanding the bonding nature of uranyl ion and functionalized graphene: A theoretical study. *J. Phys. Chem. A* **2014**, *118*, 2149−2158.

(26) Li, X.; Wang, X.; Zhang, L.; Lee, S.; Dai, H. Chemically derived, ultrasmooth graphene nanoribbon semiconductors. *Science* **2008**, *319*, 1229−1232.

(27) Cai, D.; Song, M. Preparation of fully exfoliated graphite oxide nanoplatelets in organic solvents. *J. Mater. Chem.* **2007**, *17*, 3678−3680.

(28) Zhang, L.; Xia, J.; Zhao, Q.; Liu, L.; Zhang, Z. Functional graphene oxide as a nanocarrier for controlled loading and targeted delivery of mixed anticancer drugs. *Small* **2010**, *6*, 537−544.

(29) Hummers, W. S.; Offeman, R. E. Preparation of graphitic oxide. *J. Am. Chem. Soc.* **1958**, *80*, 1339−1339.

(30) Sun, X. M.; Liu, Z.; Welsher, K.; Robinson, J. T.; Goodwin, A.; Zaric, S.; Dai, H. J. Nano-graphene oxide for cellular imaging and drug delivery. *Nano Res.* **2008**, *1*, 203−212.

(31) Hermanson, G. T. Homobifunctional crosslinkers. In *Bioconjugate techniques*; Hermanson, G. T., Ed.; Academic Press: Boston, 2013; pp 275−298.

(32) Shin, H. J.; Kim, K. K.; Benayad, A.; Yoon, S. M.; Park, H. K.; Jung, I. S.; Jin, M. H.; Jeong, H.-K.; Kim, J. M.; Choi, J. Y.; Lee, Y. H. Efficient reduction of graphite oxide by sodium borohydride and its

DOI: 10.1021/es505590j
Environ. Sci. Technol. 2015, 49, 4255−4262

effect on electrical conductance. *Adv. Funct. Mater.* **2009**, *19*, 1987−1992.
(33) Shen, J.; Hu, Y.; Shi, M.; Lu, X.; Qin, C.; Li, C.; Ye, M. Fast and facile preparation of graphene oxide and reduced graphene oxide nanoplatelets. *Chem. Mater.* **2009**, *21*, 3514−3520.
(34) Newville, M. EXAFS analysis using FEFF and FEFFIT. *J. Synchrotron Radiat.* **2001**, *8*, 96−100.
(35) Frisch, M. J.; Trucks, G. W.; Schlegel, H. B.; Scuseria, G. E.; Robb, M. A.; Cheeseman, J. R.; Scalmani, G. E.; Barone, V.; Mennucci, B.; Petersson, G. A. *Gaussian 09, Revision A.02*; Gaussian, Inc.: Wallingford, CT, 2009.
(36) Perdew, J. P.; Burke, K.; Ernzerhof, M. Generalized gradient approximation made simple. *Phys. Rev. Lett.* **1996**, *77*, 3865−3868.
(37) Balabanov, N. B.; Peterson, K. A. Systematically convergent basis sets for transition metals. I. All-electron correlation consistent basis sets for the 3d elements Sc-Zn. *J. Chem. Phys.* **2005**, *123*, 64107.
(38) Cossi, M.; Barone, V.; Robb, M. A. A direct procedure for the evaluation of solvent effects in MC-SCF calculations. *J. Chem. Phys.* **1999**, *111*, 5295−5302.
(39) Cossi, M.; Rega, N.; Scalmani, G.; Barone, V. Energies, structures, and electronic properties of molecules in solution with the C-PCM solvation model. *J. Comput. Chem.* **2003**, *24*, 669−681.
(40) Stankovich, S.; Dikin, D. A.; Piner, R. D.; Kohlhaas, K. A.; Kleinhammes, A.; Jia, Y. Y.; Wu, Y.; Nguyen, S. T.; Ruoff, R. S. Synthesis of graphene-based nanosheets via chemical reduction of exfoliated graphite oxide. *Carbon* **2007**, *45*, 1558−1565.
(41) Si, Y.; Samulski, E. T. Synthesis of water soluble graphene. *Nano Lett.* **2008**, *8*, 1679−1682.
(42) Stankovich, S.; Piner, R. D.; Nguyen, S. T.; Ruoff, R. S. Synthesis and exfoliation of isocyanate-treated graphene oxide nanoplatelets. *Carbon* **2006**, *44*, 3342−3347.
(43) Lee, D. W.; De Los Santos V, L.; Seo, J. W.; Felix, L. L.; Bustamante D, A.; Cole, J. M.; Barnes, C. H. W. The structure of graphite oxide: Investigation of its surface chemical groups. *J. Phys. Chem. B* **2010**, *114*, 5723−5728.
(44) Kumar, N. A.; Choi, H. J.; Shin, Y. R.; Chang, D. W.; Dai, L.; Baek, J. B. Polyaniline-grafted reduced graphene oxide for efficient electrochemical supercapacitors. *ACS Nano* **2012**, *6*, 1715−1723.
(45) Ramanathan, T.; Fisher, F. T.; Ruoff, R. S.; Brinson, L. C. Amino-functionalized carbon nanotubes for binding to polymers and biological systems. *Chem. Mater.* **2005**, *17*, 1290−1295.
(46) Fan, X.; Peng, W.; Li, Y.; Li, X.; Wang, S.; Zhang, G.; Zhang, F. Deoxygenation of exfoliated graphite oxide under alkaline conditions: A green route to graphene preparation. *Adv. Mater.* **2008**, *20*, 4490−4493.
(47) Sheng, Z. H.; Shao, L.; Chen, J. J.; Bao, W.-J.; Wang, F. B.; Xia, X. H. Catalyst-free synthesis of nitrogen-doped graphene via thermal annealing graphite oxide with melamine and its excellent electrocatalysis. *ACS Nano* **2011**, *5*, 4350−4358.
(48) Su, Q.; Pang, S.; Alijani, V.; Li, C.; Feng, X.; Müllen, K. Composites of graphene with large aromatic molecules. *Adv. Mater.* **2009**, *21*, 3191−3195.
(49) Ferrari, A. C.; Meyer, J. C.; Scardaci, V.; Casiraghi, C.; Lazzeri, M.; Mauri, F.; Piscanec, S.; Jiang, D.; Novoselov, K. S.; Roth, S.; Geim, A. K. Raman spectrum of graphene and graphene layers. *Phys. Rev. Lett.* **2006**, *97*, 187401.
(50) Ramesha, G. K.; Sampath, S. Electrochemical reduction of oriented graphene oxide films: An in situ Raman spectroelectrochemical study. *J. Phys. Chem. C* **2009**, *113*, 7985−7989.
(51) Szabo, T.; Berkesi, O.; Forgo, P.; Josepovits, K.; Sanakis, Y.; Petridis, D.; Dekany, I. Evolution of surface functional groups in a series of progressively oxidized graphite oxides. *Chem. Mater.* **2006**, *18*, 2740−2749.
(52) Yang, D.; Velamakanni, A.; Bozoklu, G.; Park, S.; Stoller, M.; Piner, R. D.; Stankovich, S.; Jung, I.; Field, D. A.; Ventrice, C. A., Jr.; Ruoff, R. S. Chemical analysis of graphene oxide films after heat and chemical treatments by X-ray photoelectron and Micro-Raman spectroscopy. *Carbon* **2009**, *47*, 145−152.
(53) Whitby, R. L. D.; Gun'ko, V. M.; Korobeinyk, A.; Busquets, R.; Cundy, A. B.; László, K.; Skubiszewska-Zięba, J.; Leboda, R.; Tombácz, E.; Toth, I. Y.; Kovacs, K.; Mikhalovsky, S. V. Driving forces of conformational changes in single-layer graphene oxide. *ACS Nano* **2012**, *6*, 3967−3973.
(54) Chowdhury, I.; Duch, M. C.; Mansukhani, N. D.; Hersam, M. C.; Bouchard, D. Colloidal properties and stability of graphene oxide nanomaterials in the aquatic environment. *Environ. Sci. Technol.* **2013**, *47*, 6288−6296.
(55) Wu, L.; Liu, L.; Gao, B.; Carpena, R. M.; Zhang, M.; Chen, H.; Zhou, Z. H.; Wang, H. Aggregation kinetics of graphene oxides in aqueous solutions: experiments, mechanisms, and modeling. *Langmuir* **2013**, *29*, 15174−15181.
(56) Hayes, K. F.; Papelis, C.; Leckie, J. O. Modeling ionic strength effects on anion adsorption at hydrous oxide/solution interfaces. *J. Colloid Interface Sci.* **1988**, *125*, 717−726.
(57) McBride, M. B. A critique of diffuse double layer models applied to colloid and surface chemistry. *Clays Clay Miner.* **1997**, *45*, 598−608.
(58) Goldberg, S.; Johnston, C. T. Mechanisms of arsenic adsorption on amorphous oxides evaluated using macroscopic measurements, vibrational spectroscopy, and surface complexation modeling. *J. Colloid Interface Sci.* **2001**, *234*, 204−216.
(59) Robinson, J. T.; Tabakman, S. M.; Liang, Y.; Wang, H.; Casalongue, H. S.; Vinh, D.; Dai, H. Ultrasmall reduced graphene oxide with high near-infrared absorbance for photothermal therapy. *J. Am. Chem. Soc.* **2011**, *133*, 6825−6831.
(60) Gao, W.; Alemany, L. B.; Ci, L.; Ajayan, P. M. New insights into the structure and reduction of graphite oxide. *Nat. Chem.* **2009**, *1*, 403−408.
(61) Xu, Z.; Gao, C. Aqueous liquid crystals of graphene oxide. *ACS Nano* **2011**, *5*, 2908−2915.
(62) Bargar, J. R.; Reitmeyer, R.; Lenhart, J. J.; Davis, J. A. Characterization of U(VI)-carbonato ternary complexes on hematite: EXAFS and electrophoretic mobility measurements. *Geochim. Cosmochim. Acta* **2000**, *64*, 2737−2749.
(63) Catalano, J. G.; Brown, G. E. Uranyl adsorption onto montmorillonite: Evaluation of binding sites and carbonate complexation. *Geochim. Cosmochim. Acta* **2005**, *69*, 2995−3005.
(64) Sun, Y. B.; Yang, S. T.; Sheng, G. D.; Guo, Z. Q.; Tan, X. L.; Xu, J. Z.; Wang, X. K. Comparison of U(VI) removal from contaminated groundwater by nanoporous alumina and non-nanoporous alumina. *Sep. Purif. Technol.* **2011**, *83*, 196−203.
(65) Arai, Y.; McBeath, M.; Bargar, J. R.; Joye, J.; Davis, J. A. Uranyl adsorption and surface speciation at the imogolite−water interface: Self-consistent spectroscopic and surface complexation models. *Geochim. Cosmochim. Acta* **2006**, *70*, 2492−2509.
(66) Coda, A.; Della Giusta, A.; Tazzoli, V. The structure of synthetic andersonite, $Na_2Ca[UO_2(CO_3)_3]\cdot xH_2O$. *Acta Crystallogr., Sect. B: Struct. Sci.* **1981**, *37*, 1496−1500.
(67) Glezakou, V. A.; deJong, W. A. Cluster-models for uranyl(VI) adsorption on alpha-alumina. *J. Phys. Chem. A* **2011**, *115*, 1257−63.
(68) Lan, J. H.; Cao, D. P.; Wang, W. C.; Smit, B. Doping of alkali, alkaline-earth, and transition metals in covalent-organic frameworks for enhancing CO_2 capture by first-principles calculations and molecular simulations. *ACS Nano* **2010**, *4*, 4225−4237.

DOI: 10.1021/es505590j
Environ. Sci. Technol. 2015, 49, 4255−4262